

# Deep learning based enhancement of ordered statistics decoding of short LDPC codes

Guangwen Li, Xiao Yu

**Abstract**—In the pursuit of designing highly effective decoders for short LDPC codes nearing maximum likelihood performance, we employ a relayed decoding strategy. A neural min-sum decoder initiates the decoding process, and its errors undergo postprocessing through an adaptive ordered statistics decoding. Several key initiatives supporting the latter are emphasized. Firstly, soft information at each iteration of the neural min-sum decoder is gathered and input into a convolutional neural network to enhance bit reliability estimates. This process identifies error-prone bits, either excluding them from the most reliable basis or concentrating them at the forefront, both advantageous for the adaptive ordered statistical decoding. Additionally, a decoding path, comprising a list of order patterns, directs the postprocessing process. Adjustable path length and refined constraints on associated order patterns offer diverse means of complexity management. Simultaneously, a novel auxiliary criterion is introduced to significantly reduce the list size of codeword candidates in the adaptive ordered statistics decoding. Extensive experimental results and complexity analysis validate the serial architecture, equipped with these innovations, as a formidable contender against state-of-the-art decoders for short LDPC codes.

**Index Terms**—Deep learning, Neural network, Belief propagation, Min-Sum, Training

## I. INTRODUCTION

Channel coding plays a critical role in ensuring reliable information transmission within telecommunication systems. Among linear block codes, low-density parity-check (LDPC) codes by Gallager [1] have distinguished themselves for their exceptional error correction capabilities, even approaching the theoretical Shannon limit asymptotically [2]. In domains like the Internet of things (IoT), where low complexity and minimal latency are paramount, standard iterative belief propagation (BP) decoders may yield to approximations like min-sum (MS) variants due to computational constraints [3], [4]. In contrast to the optimal Maximum Likelihood (ML) decoding, BP proves suboptimal for finite-length LDPC codes due to the presence of short cycles in the code structure. These simplified MS versions exacerbate this limitation, driving significant efforts towards narrowing this performance gap.

The ordered statistics decoding (OSD), introduced by Fosserier [5], provides an approximation of the ML decoder for short linear block codes but comes with an inherent increase in complexity. Originally proposed as a postprocessing step for LDPC codes to address decoding errors occurring intermittently during BP iterations [6], [7], it was observed that

this configuration noticeably hampers decoding throughput. Since the OSD implementation operates as a serial process, integrating it with the highly parallel iterations of BP creates a significant capacity mismatch between the two. In an effort to expedite decoding speed and reduce OSD complexity, Yue et al. [8] introduced two early stopping criteria, leveraging a devised probabilistic measure for all codeword candidates. The effectiveness of these criteria was demonstrated through simulations on BCH codes. Similarly, Yue et al. [9] aimed to mitigate OSD overhead by introducing two preconditions for invoking the binary Gaussian elimination (GE) operation. This approach resulted in substantial savings in GE workload, especially in regions of high signal-to-noise ratio (SNR), with minimal performance penalty. In a related study by Cavarec et al. [10], two sufficient or necessary conditions were integrated into the OSD when traversing its codeword candidates. This integration accelerated processing through early-stopping or skipping actions, without incurring significant performance loss.

In the last decade, the emerging field of deep learning holds tremendous promise for seamless transitions across various domains, including image processing [11], natural language processing [12], autonomous driving [13], and, most recently, error correction coding. Notably, when crafting a robust neural network (NN) decoding architecture, Nachmani et al.'s groundbreaking work [14] suggests the direct unrolling of standard BP iterations into a dedicated NN with trainable parameters for each network edge. This approach addresses the 'curse of dimensionality' in code space [15]. Without prior structural considerations, using an NN might pose challenges in accommodating the properties inherent to the code structure. To alleviate the complexity associated with tanh or inverse tanh functions in standard BP, NN adaptations of normalized min-sum (NMS) [3] and offset min-sum (OMS) decoders [4] have demonstrated remarkable decoding performance for classical block codes [16]–[21]. An intriguing approach involves employing a senior NN as a teacher, providing guidance to a new NN to enhance decoding through training [22]. Furthermore, in a study by Buchberger et al. [23], a NN was devised to identify and exclude extraneous check nodes from the overcomplete parity-check matrix  $\mathbf{H}$  in each layer, achieving a commendable balance between performance and complexity for short LDPC codes. However, extending this approach to longer codes poses a significant challenge due to the nontrivial task of finding a qualified overcomplete  $\mathbf{H}$ . In another investigation by Buchberger et al. [24], the integration of an NN to determine which variable nodes to

G.Li is with the College of Information & Electronics, Shandong Technology and Business University, Yantai, China e-mail: lgwa@sdu.edu.cn

X.Yu is with the Department of Physical Sports, Binzhou Medical University, Yantai, China e-mail: yuxiao@bzmu.edu.cn

decimate resulted in a neural BP with decimation (NBP-D), effectively ensembling multiple decoding outcomes and significantly boosting decoding performance. Nevertheless, this enhancement comes at the cost of substantially increased complexity. Addressing decoding errors in BP due to dominant absorbing sets within the LDPC code structure, a suite of recurrent neural network (RNN) models was tailored and individually trained for each type of absorbing set [25]. The amalgamation of the BP-RNN ensemble and ordered statistics decoding (OSD) was found to closely approach maximum likelihood (ML) performance for short LDPC codes, earning recognition as the state-of-the-art (SOTA) decoder. However, effective training of this scheme demands considerable effort, and its scalability to longer codes remains an area for further exploration.

Given that parallel processing of BP or any MS variant results in only a few decoding errors for the concatenated serial OSD processing, such an architecture justifies itself by largely alleviating the processing capacity mismatch concerning latency. In the pursuit of a better estimation of bit reliability, which is significantly beneficial for OSD, Jiang et al. proposed accumulating the a posteriori logarithmic likelihood ratio (LLR) of each codeword bit per iteration via weighted summing [26]. In a related approach, it was assumed that the decoding error of BP had significantly deteriorated the bit reliability. As a remedy, several BP-like iterations were initiated from scratch with the aim of yielding a new reliability metric for OSD [27]. However, this method requires prior knowledge of the noise variance, and inaccurate estimation may lead to performance degradation.

In this paper, we adopt the concatenation of NMS and OSD for the same consideration, highlighting an innovative method of synthesizing new bit reliability via a deep learning model [14]. On the other hand, despite numerous recently proposed search strategies for OSD aiming to improve efficiency through saving memory consumption or reducing computational complexity, we propose prioritizing the search order of these test error patterns (TEPs) with respect to the occurrence ratios of the order patterns they belong to in simulations. From certain perspectives, the proposed adaptive order- $p$  OSD is capable of presenting various flavors of OSD variants between conventional order- $(p-1)$  and order- $p$  OSD in terms of performance and computational complexity by adjusting some flexible parameters. Although primarily motivated by empirical statistics, the adopted combination of NMS and OSD manifests itself as a unified decoder architecture that amalgamates the advantages of low complexity, high throughput, and quasi-ML performance of short LDPC codes. Moreover, it exhibits attributes such as not requiring channel knowledge, robustness across a wide signal-to-noise ratio (SNR) range, and ease of training [22], [23].

The main contributions of this paper encompass the following items:

- \* We introduced a novel approach, decoding information aggregation (DIA), for estimating bit reliability in NMS decoding errors. Unlike conventional methods using the

magnitude of the received sequence or a posteriori LLRs of the last iteration, DIA leverages a simple convolutional neural network (CNN) trained on the complete decoding trajectory of each error bit from the NMS decoding. This significantly enhances OSD performance and holds promise for other OSD variants tailored to decoding errors from various iterative decoders.

- \* Conventional order- $p$  OSD assumes at most  $p$  error bits in the most reliable basis (MRB) for correct decoding. However, exhaustive searching through all possible TEPs in the MRB lacks statistical efficiency. We propose an Adaptive OSD that divides the MRB into three parts, defines a decoding path with a list of dominant order patterns based on error bit statistics. By controlling the path length  $l_{pt}$  or imposing additional constraints on these order patterns, we can actively adjust the trade-off between performance and complexity, especially beneficial in the cases of limited computing resources.
- \* We introduced an auxiliary criterion in the final phase of OSD to serve as a threshold for including qualified candidates in the codeword list. This criterion effectively reduces computational complexity and memory consumption by significantly reducing the list size with minimal performance degradation.
- \* The unified architecture of NMS and adaptive OSD connected by DIA between them, when integrated with the above initiatives, demonstrated comparable performance to the SOTA decoders for short LDPC codes, with significantly lower complexity in simulations. Furthermore, our scheme was extended to longer LDPC codes of more than several hundred bits, presenting decoding results not reported by its counterparts and highlighting the potential challenges associated with this extension.

The rest of the paper is organized as follows: Section II provides essential preliminaries about BP decoding variants and OSD variants. In Section III, we elaborate on the motivations behind our work. Section IV demonstrates the experimental results and complexity analysis. Finally, Section V concludes the paper with remarks and suggestions for further research.

## II. PRELIMINARIES

Given a binary row message vector  $\mathbf{m} = [m_i]_1^K$ , the encoder transforms it into  $\mathbf{c} = [c_i]_1^N$  by calculating  $\mathbf{c} = \mathbf{m}\mathbf{G}$  in  $\text{GF}(2)$ , where  $K$  and  $N$  are the lengths of the message and codeword respectively, and the generator matrix  $\mathbf{G}$  is assumed to be full-rank without loss of generality.

After the simple binary phase shift keying (BPSK) modulation maps each codeword bit  $c_i$  into one symbol  $s_i = 1 - 2c_i$ , a sequence  $\mathbf{y} = [y_i]_1^N$  with  $y_i = s_i + n_i$  is received at the channel output, where  $n_i$  denotes the channel noise with mean zero and variance  $\sigma^2$ .

Defining LLR of the  $i$ -th bit as

$$l_i = \log \left( \frac{p(y_i | c_i = 0)}{p(y_i | c_i = 1)} \right) = \frac{2y_i}{\sigma^2} \quad (1)$$

it is evident that the magnitude of  $y_i$  serves as a reliable metric for assessing the confidence in the  $i$ -th bit's hard decision  $\hat{c}_i$ , which is either '1' or '0' depending on the sign of  $y_i$ . Namely,  $\hat{c}_i = \mathbf{1}(y_i < 0)$ , where  $\mathbf{1}(\cdot)$  is the indicator function.

#### A. Standard BP and MS Variants

The bipartite Tanner graph of a code, determined by its parity check matrix  $\mathbf{H}$ , consists of  $N$  variable nodes and  $M$  check nodes connected by edges representing '1's in the  $i$ -th row and  $j$ -th column of  $\mathbf{H}$  where  $i \in \{0, 1, \dots, M-1\}$  and  $j \in \{0, 1, \dots, N-1\}$ .

For LDPC codes, standard BP is a competitive decoding scheme, optimal under the assumption of a tree-like Tanner graph without cycles. However, for finite-length codes, it becomes suboptimal due to short cycles violating the independence assumption of communicated messages.

Examining the flooding message schedule of BP, suppose  $t \in \{1, 2, \dots, T\}$ , where  $T$  is the maximum number of iterations, then the message from variable node  $v_i$  to check node  $c_j$  at the  $t$ -th iteration is given by (2):

$$x_{v_i \rightarrow c_j}^{(t)} = l_i + \sum_{\substack{c_p \rightarrow v_i \\ p \in \mathcal{C}(i)/j}} x_{c_p \rightarrow v_i}^{(t-1)} \quad (2)$$

where all  $x_{c_p \rightarrow v_i}^{(0)}$  are initialized to be zeros.

The reversed message from  $c_j$  to  $v_i$  is expressed as (3):

$$x_{c_j \rightarrow v_i}^{(t)} = 2 \tanh^{-1} \left( \prod_{\substack{v_q \rightarrow c_j \\ q \in \mathcal{V}(j)/i}} \tanh \left( \frac{x_{v_q \rightarrow c_j}^{(t)}}{2} \right) \right) \quad (3)$$

Here,  $\mathcal{C}(i)/j$  denotes all neighboring check nodes of  $v_i$  excluding  $c_j$ , and  $\mathcal{V}(j)/i$  denotes all neighboring variable nodes of  $c_j$  excluding  $v_i$ .

The a posteriori LLR of the  $i$ -th bit at the  $t$ -th iteration, whose sign determines its hard decision, is defined as (4):

$$x_{v_i}^{(t)} = l_i + \sum_{\substack{c_p \rightarrow v_i \\ p \in \mathcal{C}(i)}} x_{c_p \rightarrow v_i}^{(t-1)} \quad (4)$$

To reduce intensive computation, a simple approximation (5) is used to substitute the computation of  $\tanh$  or  $\tanh^{-1}$  functions in (3) for the MS algorithm, at the cost of some performance loss:

$$\begin{aligned} x_{c_j \rightarrow v_i}^{(t)} &= s_{c_j \rightarrow v_i}^{(t)} \omega_{c_j \rightarrow v_i}^{(t)} \quad (5) \\ s_{c_j \rightarrow v_i}^{(t)} &= \prod_{\substack{v_q \rightarrow c_j \\ q \in \mathcal{V}(j)/i}} \text{sgn} \left( x_{v_q \rightarrow c_j}^{(t)} \right) \\ \omega_{c_j \rightarrow v_i}^{(t)} &= \min_{\substack{v_q \rightarrow c_j \\ q \in \mathcal{V}(j)/i}} \left| x_{v_q \rightarrow c_j}^{(t)} \right| \end{aligned}$$

where  $\text{sgn}(\cdot)$  denotes the sign function.

As opposed to standard BP, whose decoding performance suffers from inaccurate estimation of channel noise  $\sigma^2$  [19],

another attractiveness of MS lies in its scale invariance to  $\sigma^2$ , implying no impact is expected for MS decoding when  $l_i$  in (2) is replaced by  $y_i$ .

To narrow the performance gap between MS and BP decoders, NMS or OMS were proposed to appropriately weight or offset the min term  $\omega_{c_j \rightarrow v_i}^{(t)}$  in (5).

BP, NMS, or OMS can be readily transformed into a trellis-like NN by unrolling each iteration of the decoding process, with the added complexity of imposing weights or offsets on the neural network edges. Among the NN versions of BP, NMS, and OMS, BP has the highest complexity, and OMS generally lags behind NMS [19] in terms of performance. Therefore, we prefer the simplest neural network form of NMS, where the NN edges related to the min term  $\omega_{c_j \rightarrow v_i}^{(t)}$  in (5) are all weighted with a shared parameter across iterations.

During the training phase, the neural decoder is supplied with a batch of data and assessed for its output using the standard cross-entropy loss function. Following this, a stochastic gradient descent (SGD) optimizer is employed to adjust the single parameter. The training process iterates until a stopping criterion is met, such as when the fluctuation of the loss value over several consecutive iterations falls within a predefined range. It has been observed that a well-trained NMS can effectively bridge most of the performance gaps between MS and BP.

#### B. OSD of Linear Block Codes

The OSD of linear block codes falls into two main categories: algorithms based on operations involving the parity check matrix  $\mathbf{H}$  and those involving the generator matrix  $\mathbf{G}$ . Due to the duality observed in their presentation and performance, our focus is exclusively on the former.

For  $\mathbf{H}$ -centered OSD algorithms, it is crucial to note that the bit indices of a received sequence  $\mathbf{y}$  align one by one with the column indices of the initial matrix  $\mathbf{H}^{(0)} = \mathbf{H}$ . This implies two latent interactions during the OSD processing between the sequence  $\mathbf{y}^{(i)}$  and matrix  $\mathbf{H}^{(i)}$ .

- (i) Sorting some or all bits of  $\mathbf{y}^{(i)}$  leads to the rearrangement of some or all columns of  $\mathbf{H}^{(i-1)}$  into  $\mathbf{H}^{(i)}$ .
- (ii) Requested column swaps of  $\mathbf{H}^{(i)}$  result in the rearrangement of the involved bits of  $\mathbf{y}^{(i-1)}$  into  $\mathbf{y}^{(i)}$ .

As a side note, the terms 'bit,' 'bit position,' and 'bit index' may be used interchangeably if their meanings are self-evident in the context, and the same holds for 'bit reliability' and 'bit metric.'

The conventional order- $p$  OSD follows these steps:

- 1) Sort the received sequence  $\mathbf{y}$  in ascending order based on individual bit metrics to obtain  $\mathbf{y}^{(1)}$ . Simultaneously, partition  $\mathbf{y}^{(1)}$  into two sections: the MRB consisting of the last  $K$  bits of the sorted list, and the Least Reliable Basis (LRB) comprising the remaining bits. Interaction (i) is triggered for  $(\mathbf{y}^{(1)}, \mathbf{H}^{(0)})$ , resulting in  $\mathbf{H}^{(1)}$ .
- 2) The Gaussian elimination (GE) operation, including elementary row operations and requested column swaps,

reduces  $\mathbf{H}^{(1)}$  to its systematic form  $\mathbf{H}^{(2)} = [\mathbf{I} : \mathbf{Q}_2]$ . Simultaneously, interaction (ii) is triggered for  $(\mathbf{y}^{(1)}, \mathbf{H}^{(2)})$ , yielding  $\mathbf{y}^{(2)}$ .

- 3) The hard decision of the last  $K$  bit positions of  $\mathbf{y}^{(2)}$  yields the anchoring point  $\mathbf{c}_a$  of MRB. For all  $\varpi = \sum_{i=0}^p \binom{K}{i}$ , the binary Truncated Error Pattern (TEP)  $\mathbf{e}_j = [e_i]_1^K$ ,  $j \in \{0, 1, \dots, \varpi - 1\}$ , allows at most  $p$  nonzero entries. Then,  $\bar{\mathbf{c}}_{j,2} = \mathbf{c}_a \oplus \mathbf{e}_j$  serves as the  $j$ -th estimate of the MRB. Due to the parity check constraint of (6), a codeword candidate  $\bar{\mathbf{c}}_j = [\bar{\mathbf{c}}_{j,1} : \bar{\mathbf{c}}_{j,2}]$  is secured.

$$\mathbf{H}^{(2)} \bar{\mathbf{c}}_j^T = \mathbf{0} \Rightarrow \bar{\mathbf{c}}_{j,1} = \bar{\mathbf{c}}_{j,2} \mathbf{Q}_2 \quad (6)$$

where the derived  $\bar{\mathbf{c}}_{j,1}$  denotes the  $j$ -th estimate of the LRB.

- 4) The list of codeword candidates  $\bar{\mathbf{c}}_j$ ,  $j \in \{0, 1, \dots, \varpi - 1\}$ , competes for the optimal estimate under the criterion:

$$\bar{\mathbf{c}} = \arg \min_{\bar{\mathbf{c}}_j = [c_i]_1^N} \sum_{i=1}^N \mathbf{1}(\check{c}_i \neq c_i) \left| y_i^{(2)} \right| \quad (7)$$

where  $\check{c}_i$  is the hard decision of  $y_i^{(2)}$  (the  $i$ -th entry of  $\mathbf{y}^{(2)}$ ).

- 5) Finally, by reversing all the involved bit swaps for  $\bar{\mathbf{c}}$ , obtain the estimated codeword  $\hat{\mathbf{c}}$  for the received sequence  $\mathbf{y}$  and parity check matrix  $\mathbf{H}$ . < end >

### III. MOTIVATIONS

#### A. DIA Model

1) *Rationale of DIA*: The efficacy of OSD heavily relies on the precise selection of  $K$  dependable bits from a given sequence to populate the MRB. This strategic selection aims to minimize the inclusion of erroneous bits. As a result, the critical challenge lies in establishing a reliable estimation for the bits within the MRB section.

Traditionally, the reliability of the  $i$ -th bit is assessed based on either its original magnitude  $|y_i|$  or the magnitude  $|x_{v_i}^{(T)}|$  in (4) as observed in the final decoding iteration of the NMS decoding process. However, it's important to note that the NMS decoder furnishes a posteriori LLR for each codeword bit in every decoding iteration, as defined by (4). Intuitively, the collection of these values forms a decoding trajectory for a given bit. Remarkably, even in cases of decoding errors of NMS, this trajectory tends to closely approximate the ground truth. Consequently, for the context of NMS decoding errors, discarding the intermediate iteration information and retaining only the data from the original or the final iteration of NMS is considered inadequate in terms of information utilization. This limitation may potentially hinder the assessment of bit reliability as input to OSD. Recognizing this, we are inclined to address this issue by aggregating information from the entire iterative decoding process to enhance the estimation of bit reliability, rather than relying solely on a specific iteration.

To achieve the objective of DIA, we turn to a class of established deep learning models. One solution, among others, involves the utilization of CNNs, renowned for their rapid

responsiveness and high-level abstraction capabilities. In the following, we will provide an illustrative example of how to implement DIA for the CSDSS LDPC (128,64) code [21].

2) *Architecture of DIA Model*: Let  $T = 12$  in our scenario. For each decoding error, the decoding trajectory of its  $i$ -th bit is treated as a time series, with a length of  $T + 1$  accounting for the received  $y_i$ . This transforms the bit reliability estimation into a time series forecasting issue.

To address this, we employ a simple CNN architecture, consisting of three 'Conv1D' layers and one 'dense' layer from the Keras package [28]. These layers are meticulously configured with parameters such as 'kernel\_size=3', 'strides=1', 'padding=valid', 'activation=linear', etc., as illustrated in Fig. 1. In this architecture, a stack of '3x1' filters slides over the decoding trajectory, extending the receptive field of bit information for the current iteration to neighboring iterations, facilitating information exchange. With more concatenated 'conv1d' layers, the receptive field continues to grow. Finally, the 'dense' layer merges all information to provide a global estimate of the current bit reliability.

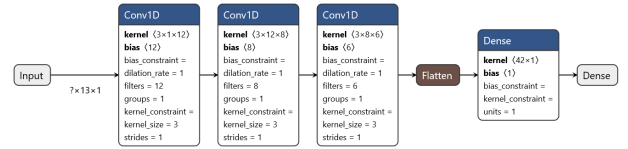


Fig. 1: CNN architecture of the DIA model for CCSDS LDPC (128,64) code with  $T = 12$

The deployment of DIA is instrumental in synthesizing a more refined reliability estimation. It operates akin to time series forecasting by capturing inherent modes and tendencies in the data.

3) *Training Logistics of DIA Model*: The training data is derived from the recorded a posteriori LLRs per iteration for all decoding errors in the NMS decoding process. In mini-batch mode, a typical input can be represented as a matrix of shape  $N \times (T + 1)$ . Here, the  $i$ -th row corresponds to the trajectory or time series for the codeword's  $i$ -th bit, and the  $j$ -th column denotes the LLRs for the  $j$ -th iteration of NMS decoding.

For optimization, we employ an SGD optimizer, such as the Adam optimizer [29], to update the trainable parameters in mini-batch mode. This process aims to minimize the cross-entropy loss function (8), defined as follows:

$$\ell_{ce}(\mathbf{c}, \hat{\mathbf{c}}) = \sum_{i=0}^{N-1} \sum_{j=0}^1 \left( p(c_i = j) \cdot \log \frac{1}{p(\hat{c}_i = j)} \right) \quad (8)$$

where  $p(c_i = j)$  takes values of 0 or 1 depending on the ground truth, and  $p(\hat{c}_i = j)$  represents the derived probability from the CNN output of the  $i$ -th bit in the form of LLR. Notably, the probability and corresponding LLR can only be derived from each other when  $\sigma^2$  is known. Thus,  $\sigma^2$  is assumed to be known by default during the training phase. During the testing phase, two crucial points merit attention.

Firstly, the cross-entropy calculation of (8) is now considered unnecessary. Secondly, the output of DIA exclusively serves as evidence for the reordering of a sequence of bits in the OSD. Thus, the relative values among the sequence bits, rather than their actual values, hold more meaningful significance. It has been verified that, despite the input to NMS being  $y_i$ , the trajectory of NMS decoding error can be effectively treated as an LLR approximation to DIA, resulting in a satisfactory estimation of bit reliability.

Given that the adopted model is relatively simple and has only a small number of trainable parameters, it exhibits low sensitivity to the choice of the learning rate, set initially to 0.01. As anticipated, the model's training quickly converges after approximately 1000 steps, demonstrating a stable loss value within minutes, even when run on a standard personal computer.

4) *Impact of DIA Model on NMS Decoding Errors:* For the LDPC (128,64) code, we conduct a comprehensive analysis of the impact of the DIA model on the decoding errors of NMS from two crucial perspectives.

- As presented in Table I, we evaluate the frame error rate (FER), bit error rate (BER), and cross-entropy metrics of decoding errors under diverse conditions at SNR=2.8dB. The results underscore two key advantages of the DIA model. Firstly, the superior BER of DIA implies fewer erroneous bits in the MRB of OSD, thereby increasing the likelihood of being covered by a lower order- $p$  OSD. Secondly, the cross-entropy of DIA (23.10) significantly outperforms the evaluations of the  $T$ -th NMS iteration (38.70) or the received sequence (49.44). This improvement signifies a substantial enhancement in the average bit reliability evaluation. In simpler terms, the DIA output instills more confidence in the bits selected in the MRB of OSD for its hard decisions. Even if a wrong hard decision occurs in the MRB, it is more likely to happen in the foremost part of MRB compared to the other two measurements. This observation motivates our adaptive OSD to leverage this concentration effect. Similar observations can be made at SNR=3.2dB.

TABLE I: Comparison of FER, BER, and cross-entropy for NMS decoding errors of the (128,64) code at different iterations and with DIA.

SNR	FER	BER	Cross-entropy
2.8dB	1.0/1.0/0.98	0.111/0.0827/ <b>0.074</b>	49.44/38.70/ <b>23.10</b>
3.2dB	1.0/1.0/0.98	0.107/0.0735/ <b>0.066</b>	49.38/36.82/ <b>20.99</b>

- The input of OSD may be the output of DIA model or the LLRs at the  $T$ -th iteration of NMS decoding etc., thus to identify the efficacy of DIA model, we are intrigued to sort the OSD input to acquire the distribution of the number of erroneous bits in its MRB, termed the live error bit count  $\delta$ , since the decoding error is decodable only when  $\delta \leq p$  for an order- $p$  OSD.

For the simulations of (128,64) code at SNR=2.8dB and 3.5dB, Fig. 2 shows the relative frequency (RF) his-

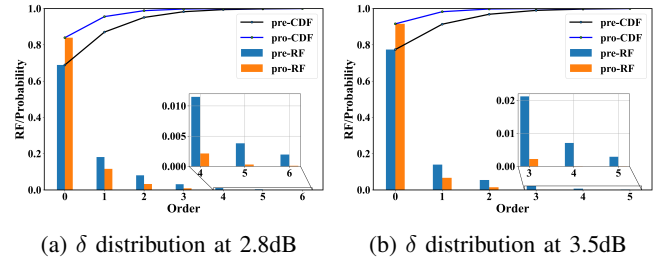


Fig. 2: Distributions of live error bit count  $\delta$  for NMS decoding errors of (128,64) code at different SNRs with and without DIA.

tograms after collecting the occurrences of  $\delta$  by making hard decisions on the LLRs of the  $T$ -th iteration of NMS decoding and DIA model output separately, noted as 'pre' and 'pro' in the legend, with their cumulative distribution function (CDF) curves included as well. It reveals small  $\delta$  cases account for most decoding errors for both metrics, and DIA consistently outperforms its rival in both SNRs, which is also suggested by the fact CDF curve for DIA always stays above that for absence of it. This insight can also be obtained by examining the more detailed RFs of each  $\delta$  evaluation at both SNRs in Table II.

Furthermore, the range of possible  $\delta$  evaluations shrinks with the involvement of DIA. For instance, at SNR=2.8dB, it diminishes from [0,9] to [0,7] as shown in Table II. Additionally, the heavy-tail phenomenon is significantly alleviated by DIA, echoing the concentration effect mentioned earlier.

TABLE II: Comparison of the RFs of occurrences of  $\delta$  evaluation for NMS decoding errors with and without DIA in the simulation of (128,64) code.

SNR	DIA	RF
2.8dB	No	{0: 0.68914, 1: 0.18141, 2: 0.08063, 3: 0.03155, 4: 0.0115, 5: 0.00382, 6: 0.00153, 7: 0.00036, 8: 5e-05, 9: 3e-05}
	Yes	{0: <b>0.83953</b> , 1: <b>0.1162</b> , 2: <b>0.03274</b> , 3: <b>0.00898</b> , 4: <b>0.00214</b> , 5: <b>0.00031</b> , 6: <b>8e-05</b> , 7: <b>3e-05</b> }
3.5dB	No	{0: 0.77411, 1: 0.13978, 2: 0.05487, 3: 0.02123, 4: 0.0071, 5: 0.00187, 6: 0.00067, 7: 0.00022, 8: 7e-05, 9: 7e-05}
	Yes	{0: <b>0.91591</b> , 1: <b>0.0669</b> , 2: <b>0.0148</b> , 3: <b>0.00224</b> , 4: <b>7e-05</b> , 5: <b>7e-05</b> }

## B. Decoding Path-Based Adaptive OSD

First of all, we may interchangeably refer to the MRB section from the output of the DIA model with the term 'decoding error' in context, unless explicitly stated otherwise.

While it is known that, given a sufficiently high order- $p$ , OSD can achieve ML decoding performance, the primary challenge arises from the exponentially growing complexity associated with enumerating all codeword candidates and choosing the optimal estimation as  $p$  increases. The conventional order- $p$  OSD employs a straightforward exhaustive search to populate the codeword candidates list. However, this approach lacks efficiency in terms of computation and memory consumption. This inefficiency partly stems from the

assumption that all TEPs of OSD are of equal probabilities, resulting in equal-probability codeword candidates.

Two critical considerations challenge this assumption. Firstly, the MRB bits exhibit increasing bit reliability from left to right after sorting in ascending order. Secondly, during the reduction of  $\mathbf{H}$  to its systematic form via GE operations, column swapping between MRB and LRB is commonly employed, inevitably leading to a degradation of the average bit reliability of MRB. Consequently, the uneven error likelihood for the hard decisions of MRB bits implies that the bonded TEPs bear no equal probability either. This insight forms the basis for our scheme of partitioning the MRB to enhance searching efficiency. In essence, we prioritize various TEPs, aiming to obtain the best performance by intercepting and retaining only the stack of the most promising TEPs according to individual priority when given limited computing resources. This approach is expected to achieve a better performance and complexity trade-off.

Specifically, the MRB is divided into three regions labeled LR, MR, and HR. After assigning a threshold  $\lambda_i, i \in \{1, 2, 3\}$  that regulates the exact Hamming weight of the current region, we obtain a specific mode of MRB termed order pattern. By varying the threshold in the range of  $\lambda_{im}, i \in \{1, 2, 3\}$  correspondingly, we generate a list of order patterns and denote it as a decoding path. The dominant order patterns are scheduled at the list head based on the statistics about occurrences of decoding errors whose hard decisions populate the individual order pattern through simulations. In this way, a fixed decoding path is established to be exploited in the test phase by traversing its members sequentially to generate TEPs, instead of using exhaustive searching. Furthermore, it is adjustable in terms of complexity management by tweaking the decoding path length  $l_{pt}$ , namely the number of order patterns included, or imposing more constraints on individual order patterns to allow them in the decoding path or not.

Therefore, our alternative substitutes a hierarchical-like searching approach that emphasizes putting priority on the most likely TEPs compared with the conventional approach, which simply stacks the TEPs in terms of the Hamming weight. Two pieces of supportive evidence in simulations are presented regarding the statistics about the distributions of requested swap counts in GE and order patterns.

1) *Distribution of Requested Swap Counts*: Column swapping is a common occurrence during Gaussian elimination (GE) when reducing  $\mathbf{H}$  to its systematic form. Let  $n_{sw}$  denote the number of swaps between the MRB and the LRB. Examining its distribution is crucial as it provides insights into how to reasonably partition the MRB into three regions. This partitioning result indirectly impacts the constituents of the decoding path and, consequently, the decoding performance. It's worth noting that another round of sorting is necessary for the MRB bits to be arranged in ascending order due to the related swaps in the GE operations.

As illustrated in Fig. 3, the average  $n_{sw}$  remains approximately constant at 4 for the (128,64) code, regardless of SNR=2.8dB or 3.5dB. We anticipate that  $n_{sw}$  will alter with

varied code block lengths and code rates, besides  $\mathbf{H}$ . When it comes to MRB partitioning, a conflicting reality emerges. On one hand, it's beneficial to accommodate more cases in an enlarged LR region considering the existence of the concentration effect. On the other, an oversized LR region, once assigned a higher threshold, it may deviate the aim of effectively controlling the search complexity. Hence, we suggest setting two partition points  $\alpha_1 n_{sw}$  and  $\beta_1 n_{sw}$  for the MRB respectively, where the evaluations of  $\alpha_1, \beta_1$  depend on the chosen code. For instance, for the (128,64) code,  $\alpha_1 = 1, \beta_1 = 2$  enables the MRB range of  $[0, 63]$  to be divided into  $[0, 3] \cup [4, 11] \cup [12, 63]$ .

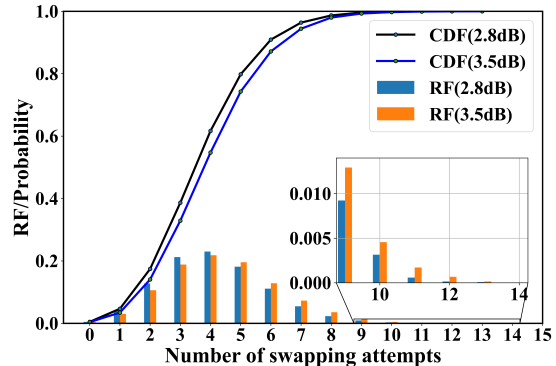


Fig. 3: Distribution of swap counts between the MRB and the LRB when reducing  $\mathbf{H}$  to its systematic form for decoding errors of (128, 64) code at SNR=2.8, 3.5 dB

2) *Distribution of Order Patterns*: Once the sizes of the LR, MR, and HR regions of MRB are determined, the order patterns can be distinguished from each other by labeling their thresholds as  $[\lambda_1, \lambda_2, \lambda_3]$ . TEPs with Hamming weights equal to  $\lambda_1, \lambda_2$ , and  $\lambda_3$  in their respective regions will be categorized into this specific order pattern. As each TEP maps to a unique codeword candidate, enumerating all possible TEPs populates the codeword candidates list.

Another consideration is how to prioritize the order patterns composing the decoding path. Our proposed solution relies on empirical results, assuming that statistics about the distribution of hard decisions in decoding errors should reflect the distribution of dominant order patterns with sufficient training samples.

Considering the (128,64) code, with or without the assistance of DIA, Table III enumerates the potential dominant order patterns for the decoding path with  $l_{pt} = 20$ . The table includes the varied ratios of respective order patterns, obtained by collecting the cases of underlying decoding errors individually. Clearly, more decoding errors are categorized into fewer dominant order patterns with the assistance of DIA. At SNR=3.0dB, a total ratio of 0.0086 decoding errors falls out of the scope of OSD with  $l_{pt} = 20$  without DIA. In contrast, the risk reduces to 0.0004 with DIA, ensuring a substantial gain. For a small  $l_{pt}$ , such as 2, with the presence of DIA, the ratio sum of '[0,0,0]' and '[1,0,0]' will yield 0.9362, representing the probability of a decoding error being

corrected. In comparison, the probability drops to 0.8299 without DIA, illustrating the concentration effect of DIA. A similar observation holds true for other varied  $l_{pt}$ .

Nevertheless, even in the absence of DIA, as shown in Table III, its decoding path is nearly identical to the case with DIA, with some permutations among their members.

Moreover, the decoding of the conventional order- $p$  OSD adheres to a special decoding path in our view. For instance, conventional order-1 OSD follows the unaltered list of order patterns of '[0,0,0]', '[1,0,0]', '[0,1,0]' and '[0,0,1]', so it presents equivalent performance and complexity as our adaptive OSD with  $l_{pt} = 4$ , including the same order patterns. However, the rigidity in terms of  $l_{pt}$  evaluation and order patterns layout hinders its applications where limited computing resources are available. To narrow the corresponding performance gap or alleviate the exponentially growing complexity, such as from order-2 OSD to higher order- $p$  OSD for codes with block lengths over 100, the adaptive OSD can effectively tailor a better trade-off between quasi order- $p$  OSD performance and significantly reduced complexity among many options.

For better complexity control, putting more constraints on these maximum limits  $\lambda_{im}$  can influence the chosen order patterns of the decoding path. For instance, in the case of the presence of DIA, the constraints  $[\lambda_{1m}, \lambda_{2m}, \lambda_{3m}] = [3, 2, 1]$  and  $\lambda_m = \sum_{i=1}^3 \lambda_{im} = 3$ , will filter out the order patterns of '[3,1,0]', '[4,0,0]' and '[2,2,0]' etc. from the decoding path shown in Table III, even with the nominal  $l_{pt} = 20$ . In comparison, with the absence of DIA, a similar result is returned under the same constraints. Deviating slightly, in the context of adaptive OSD, order- $p$  is replaced by order- $\lambda_m$  for notation convenience.

Further simulations demonstrated the chosen decoding path's near-universal applicability across a wide range of SNR regions of interest. Furthermore, the decoding path derived for one specific code may perform well for other codes without the need for identification from scratch.

The adaptive OSD, equipped with a decoding path of a variable  $l_{pt}$ , and an open mechanism for adding constraints on the affiliated order patterns, can readily surpass conventional order- $p$  OSD in terms of complexity control. Due to its exceptional flexibility and precision in customization and fine-tuning capabilities, the adaptive OSD allows for accurate estimation of the necessary computing resources to achieve a desired decoding performance, and vice versa.

TABLE III: Statistics about the distribution of order patterns when identifying the decoding path for the decoding errors of (128,64) code

SNR	DIA	Order patterns:ratio
3.0dB	No	{ '[0 0 0]': 0.6847, '[1 0 0]': 0.1452, '[2 0 0]': 0.0449, '[0 1 0]': 0.0351, '[1 1 0]': 0.0269, '[2 1 0]': 0.0125, '[3 0 0]': 0.0117, '[0 0 1]': 0.006, '[1 0 1]': 0.005, '[1 2 0]': 0.0049, '[0 2 0]': 0.0039, '[3 1 0]': 0.0037, '[2 0 1]': 0.0028, '[4 0 0]': 0.0025, '[2 2 0]': 0.0024, '[0 1 1]': 0.0024, '[1 1 1]': 0.0024, '[2 1 1]': 0.0012, '[3 2 0]': 0.001, '[3 0 1]': 0.0009 } Others: 0.0086
	Yes	{ '[0 0 0]': 0.8205, '[1 0 0]': 0.1157, '[0 1 0]': 0.0215, '[2 0 0]': 0.0197, '[1 1 0]': 0.009, '[3 0 0]': 0.0033, '[0 0 1]': 0.0029, '[2 1 0]': 0.0019, '[1 0 1]': 0.0012, '[0 2 0]': 0.0011, '[1 2 0]': 0.0007, '[0 1 1]': 0.0005, '[3 1 0]': 0.0004, '[1 1 1]': 0.0003, '[2 0 1]': 0.0003, '[4 0 0]': 0.0003, '[2 2 0]': 0.0003, '[0 3 0]': 0.0001, '[1 2 1]': 0.0001, '[5 0 0]': 0.0001 } Others: 0.0004

3) *Adaptive OSD Algorithm*: The pseudo-code for the adaptive OSD algorithm is outlined in Alg. 1, with modified portions highlighted in blue, while unaltered operations remain in black. For additional context and comparison, interested readers can refer to the conventional order- $p$  OSD described in Section II.

In summary, three sequence bit rearrangement operations transform the MRB bits into their final form  $[\tilde{y}_i^{(3)}]_{M+1}^N$ , with a focus on placing more error-prone bits in the LR region during the final sorting operation.

Compared to  $\lambda_{2m}$  or  $\lambda_{3m}$  settings, a relatively higher value is assigned to  $\lambda_{1m}$  for the sake of allowing more inclusion of decoding errors within the decodable domain, while at the cost of manageable increased complexity considering the small size of the LR region.

Among other steps, steps 5, 6, and 8 are dedicated to determining qualified order patterns for the decoding path and generating the corresponding TEPs. Step 9 introduces an auxiliary criterion, detailed in the next subsection, to further suppress computational complexity. Importantly, when viewed from a vector computing perspective, the 'repeat' block between steps 8 and 12, along with step 15 in finding the optima, can be efficiently implemented by leveraging tensor operations.

### C. Auxiliary Criterion for Downsizing the Codeword Candidates List

During the decoding process, the column swapping induced by GE operations in reducing  $\mathbf{H}$  results in some bits from the LRB and an equal number of bits from the MRB being swapped. The bits introduced into the MRB are inherently less reliable than the bits exchanged into the LRB in terms of their magnitudes. After applying a hard decision to both, it is expected that the number of erroneous bits in the former will probabilistically be more than that in the latter. Leveraging this fact allows us to reduce the size of the codeword candidate list of OSD by raising the threshold for inclusion, ultimately saving the required computing resources for subsequent processing. However, due to the unknown ground truth of bit signs, we introduce an alternative assessment termed auxiliary criterion 9.

$$\sum_{l=1}^{\psi_2(n_{sw})} \left\{ c^{(l)} \right\} \oplus \left\{ \bar{c}_{1j}^{(l)} \right\} \leq \psi_1(\lambda_m) \quad (9)$$

Here,  $\psi_1(\lambda_m)$  and  $\psi_2(n_{sw})$  are code-dependent hyper-parameters influenced by  $\lambda_m$  and  $n_{sw}$ , respectively. These parameters must be determined through experimental results.  $c^{(l)}$  refers to the hard decision of bits drawn from the LRB with the highest  $\psi_2(n_{sw})$  magnitudes, whose indices determine the selected bits in  $\bar{c}_{1j}$  in Alg. 1. Notably, the chosen bits are commonly not consecutively neighbored in positions due to the lack of sorting in the LRB to deal with column swapping. For the (128,64) code,  $\psi_1(\lambda) = 3$  and  $\psi_2(n_{sw}) = 2n_{sw}$  are evaluated in simulations.

**Algorithm 1** Order- $\lambda_m$  Adaptive OSD Algorithm

**Input:** Received sequence  $\mathbf{y}$ , Parity check matrix  $\mathbf{H}$ , Reliability metric  $\tilde{\mathbf{y}} = [\tilde{y}_i]_1^N$  from DIA output, Predetermined decoding path of length  $l_{pt}$ , and all constraints for threshold limits  $[\lambda_{1m}, \lambda_{2m}, \lambda_{3m}]$ .

**Output:** Optimal codeword estimate  $\hat{\mathbf{c}}$

- 1: Sort  $[\tilde{y}_i]_1^N$  in ascending order of magnitude to obtain  $[\tilde{y}_i^{(1)}]_1^N$ . Simultaneously,  $\mathbf{H}^{(0)} = \mathbf{H}$  transforms into  $\mathbf{H}^{(1)}$ .
- 2: Reduce  $\mathbf{H}^{(1)}$  to its systematic form  $\mathbf{H}^{(2)}$ . The requested column swapping leads to the rearrangement of  $[\tilde{y}_i^{(1)}]_1^N$  bits into  $[\tilde{y}_i^{(2)}]_1^N$ .
- 3: Sort the MRB bits of  $[\tilde{y}_i^{(2)}]_1^N$  in ascending order to obtain  $[\tilde{y}_i^{(3)}]_1^N$ , and  $\mathbf{H}^{(2)}$  transforms into its systematic form  $\mathbf{H}^{(3)} = [\mathbf{I} : \mathbf{Q}_2]$ .
- 4: Obtain the hard decision  $\mathbf{c}_a$  of  $[\tilde{y}_i^{(3)}]_{M+1}^N$  as the anchoring point.
- 5: **for**  $l \in \{1, 2, \dots, l_{pt}\}$  **do**
- 6:     **if** the  $l$ -th order pattern satisfies the constraints of  $[\lambda_{1m}, \lambda_{2m}, \lambda_{3m}]$  **then**
- 7:         **repeat:**
- 8:             Generate a TEP  $\mathbf{e}_j$  qualified for the  $l$ -th order pattern, and  $\mathbf{e}_j \oplus \mathbf{c}_a \Rightarrow \bar{\mathbf{c}}_{2j}$ ,  $\bar{\mathbf{c}}_{1j} = \mathbf{Q}_2 \bar{\mathbf{c}}_{2j}$
- 9:             **if** the criterion 9 is met **then**
- 10:                 Append the candidate  $\bar{\mathbf{c}}_j = [\bar{\mathbf{c}}_{1j} : \bar{\mathbf{c}}_{2j}]$  into the codeword candidates list.
- 11:             **end if**
- 12:         **until** traversal ends
- 13:     **end if**
- 14: **end for**
- 15: Select the optimal  $\tilde{\mathbf{c}}$  in the list akin to criterion 7, then reverse all the involved bit swaps for  $\tilde{\mathbf{c}}$  to obtain  $\hat{\mathbf{c}}$ .
- 16: **return** the estimated codeword  $\hat{\mathbf{c}}$  for  $\mathbf{y}$ .

The effectiveness of this auxiliary criterion is verified in the subsequent section's complexity analysis.

#### IV. EXPERIMENTAL RESULTS AND COMPLEXITY ANALYSIS

##### A. Parameter Settings of Codes

Assuming the NMS and DIA models have been well-trained, the decoding path for the adaptive OSD is secured, and other hyperparameters related to OSD are listed in Table IV.

TABLE IV: Settings of various hyperparameters for all tested codes

Codes	$T$	$l_{pt}$	$\lambda_m$	$\lambda_{1m}/\lambda_{2m}/\lambda_{3m}$
(64,32)	8	20	0/1	1/1/1
(96,48)	10	20	3	3/3/2
(128,64)	8/12	5/12/20	3	3/3/2
(1056,880)	20	6/12	3	3/3/2
BCH(63,36)	6	20	3	3/3/2

The decoding performance of five linear block codes will be discussed, including four LDPC codes of short to moderate

block lengths: (64,32) code, TU KL (96,48) code, CCSDS (128,64) code, WiMAX (802,16), (1056,880) code, all of rate 0.5, and one classical linear block code, BCH (63,36) code of rate 0.57. The parity check matrix in the *.alist* format and ML performance of each code can be found in the literature [21], [25].

All experiments are carried out on the TensorFlow platform, and the source code can be retrieved on GitHub at a later time.

##### B. Flow Chart of the NMS-DIA-OSD Decoding Process

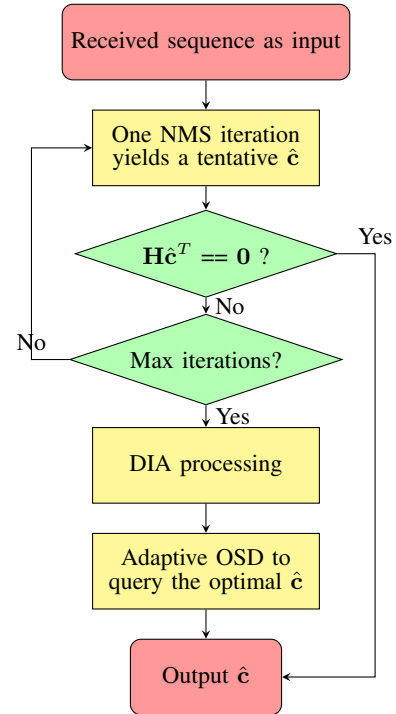


Fig. 4: Decoding of NMS-DIA-OSD architecture

As illustrated in the block diagram 4, NMS decoding can process received sequences in batch mode. Meanwhile, the early stopping criterion, once met, will terminate the entire decoding process immediately. For the collected trajectories of these NMS decoding errors, they are merged via DIA to synthesize better reliability estimates for each sequence bit, which will be subsequently fed into the adaptive OSD to start off its postprocessing.

One attractiveness of the NMS-OSD serial architecture is that the limited capacity of OSD, due to its sequential processing nature when fed with a small load of decoding errors, matches well with the parallelizable NMS fed with the bulk of the load to be processed. Considering the DIA model is parallelizable as well, the proposed NMS-DIA-OSD architecture can largely retain the characteristics of high throughput and low latency, among others.

##### C. Decoding Performance

It is a well-known fact that with a sufficiently high order  $p$ , the conventional OSD can achieve the ML performance of the

code. However, the true challenge lies in the escalating complexity and memory consumption, making it quickly infeasible with increased code block length, even if it is just above 100, which falls within the range of short LDPC codes. Therefore, the focus of the following simulation is either to achieve better decoding performance given limited complexity or to retain the same decoding performance at the cost of minimal complexity.

In our architecture, the maximum number of iterations  $T$  impacts both the NMS decoding performance and the layout of the DIA model layers. A larger  $T$  commonly yields better FER for the NMS, leaving fewer decoding errors for the OSD. However, it may result in longer latency for NMS in the worst cases and more implementation complexity for the DIA model, subsequently impacting the adaptive OSD performance. Hence, choosing a rational  $T$  evaluation involves a trade-off between performance and complexity.

In the legend of the following plots, a typical N-D-O-2(8,20) denotes the concatenation of NMS with  $T = 8$  iterations, DIA, and the adaptive OSD with  $\lambda_m = 2, l_{pt} = 20$ . As benchmarks, the decoding curves of NMS and BP alone are commonly included in the plots as well. At each SNR point under test, at least 100 decoding errors are collected to ensure plot stability. As a side note, though undetected decoding errors are observed in the simulations of very short block codes decoding, their occurrences are negligible in the waterfall SNR region of interest, thus safely ignored with no impact on our conclusions.

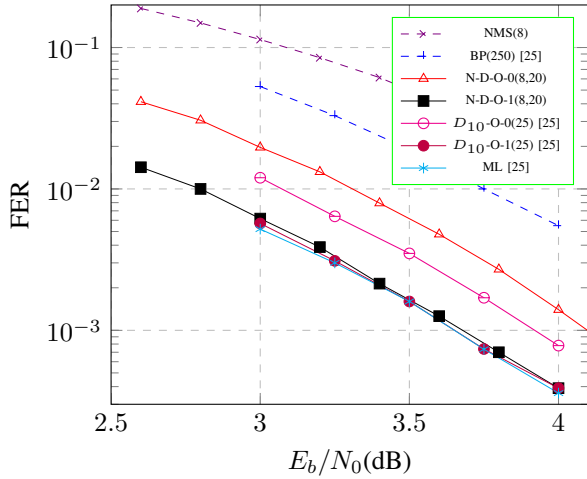


Fig. 5: FER comparison for the various proposed and SOTA decoding schemes of short (64,32) LDPC code

As shown in Fig. 5, although the proposed N-D-O-0(8,20) lags behind  $D_{10}$ -O-0(25) by about 0.2dB at  $\text{FER}=10^{-3}$ , it catches up with the latter when both upgrade to higher order 2, reaching the ML performance of the code. Notably, the true decoding path length after given the nominal  $l_{pt}$  actually depends on the number of qualified order patterns after checking the related constraints.

For a longer LDPC (96,48) code, as depicted in Fig. 6, in terms of FER performance, the proposed N-D-O-2(10,20) leads N-D-O-1(10,20) by about 0.25dB at  $\text{FER}=10^{-3}$  and

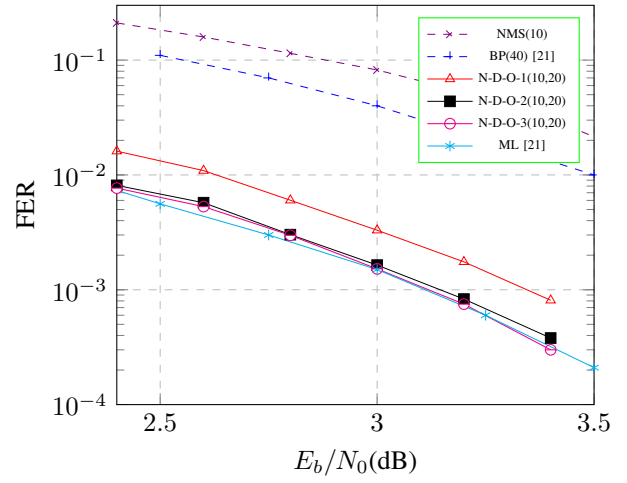


Fig. 6: FER comparison for the various proposed decoding schemes of short (96,48) LDPC code

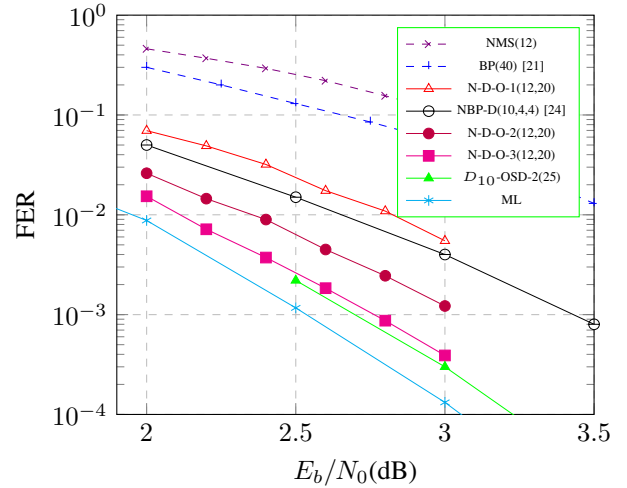


Fig. 7: FER comparison for various decoding schemes of (128,64) code

closely approaches the N-D-O-3(10,20) curve, both reaching ML performance in the waterfall SNR region. Hence, N-D-O-2(10,20) is more favored considering its significantly less complexity.

When the code block length continues to grow into 128, the required computational resources impose a hard core for our existing platform before approaching the ML performance, as shown in Fig. 7. The proposed N-D-O-3(12,20), though comparable to the SOTA  $D_{10}$ -O-2(25), both still lag behind the ML curve by within 0.2dB. Compared with other counterparts, they substantially lead NBP-D(10,4,4) [24] by beyond 0.6dB, and the latter only weakly leads the proposed order-1 combination and lags the order-2 combination by about 0.35dB at  $\text{FER}=10^{-3}$ .

To assess the scalability of our proposed scheme, we conducted simulations with a longer LDPC (1058, 880) code. Enhancing decoding for longer codes poses more challenges

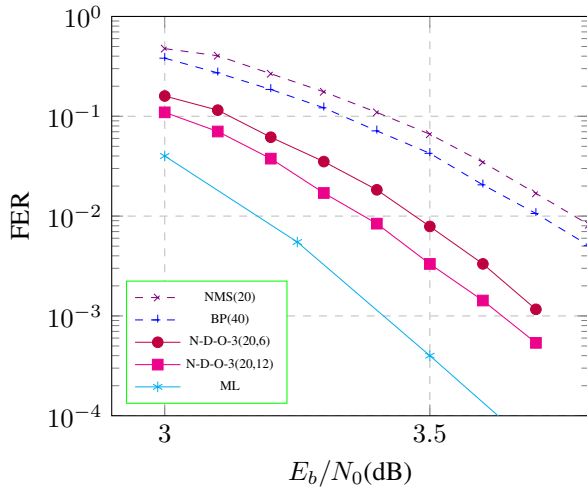


Fig. 8: Performance comparison for various decoding schemes of (1056,880) code

due to several factors. Firstly, there are more classes of order patterns solicited by the adaptive OSD to ensure targeted decoding performance. This is a consequence of decoding errors being scattered more dispersively without a prominent concentration effect for longer codes. Secondly, the escalating complexity of the conventional order-3 OSD, though far from achieving ML performance, renders its implementation unbearable. This complexity also affects the adaptive OSD, albeit in a much milder way. To address this, at the cost of some performance degradation, we employ a strategy that lowers the  $\lambda_m$  and  $l_{pt}$  settings and refines the constraints on order patterns, hoping to abandon the computation-intensive ones to curb the complexity soaring.

Fig. 8 presents the effect of varied length  $l_{pt}$  on FER performance. It is observed that the low-complexity NMS of  $T = 20$  lags behind BP decoding of  $T = 40$  by about 0.1dB. However, when combined with DIA and adaptive OSD of  $l_{pt} = 6$ , the N-D-O combination surpasses the latter significantly. Another 0.1dB performance gain is observed when  $l_{pt}$  increases to 12 for the combination. Regrettably, though there is still a 0.3dB gap from the ML curve, any attempt to narrow the gap by further increasing the  $l_{pt}$  of the adaptive OSD will incur soaring complexity, as the order patterns to be allowed in the decoding path commonly have higher threshold  $\lambda_i$ , requiring intense computation for any of them.

In comparison, with an increased code block length, the existing SOTA decoder [25] faces similar challenges from the improvement dilution effect due to expanded counts of absorbing sets. This confines its applicability only to short block lengths around 100 to acquire ML performance.

#### D. Ablation Analysis of DIA

For the LDPC (128,64) code, as depicted in Fig. 9, 'PB-NBP  $D_1$ ' [23] achieves its low-complexity target at the cost of a significant performance degradation, while NBP-D(10,4,4)

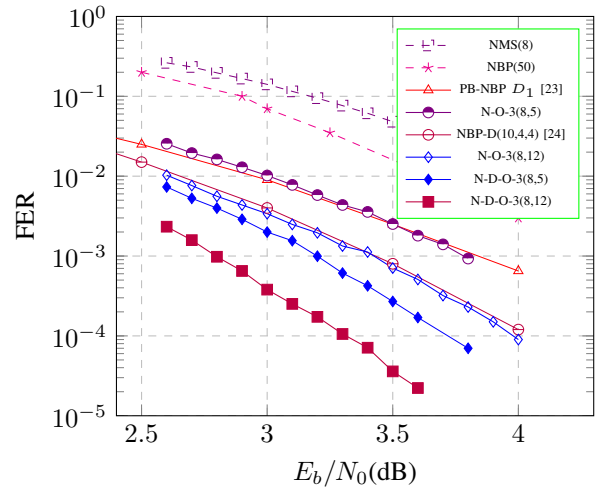


Fig. 9: FER comparison of various decoders of LDPC (128,64) code for the ablation of DIA

[24] demonstrates comparable performance to N-O-3(8,12) in terms of FER. Notably, compared with individual counterparts, an observed gain of at least 0.3dB is evident for  $l_{pt} = 5$  or  $l_{pt} = 12$  with the presence of DIA, indicating that improved bit reliability estimates can significantly boost OSD performance.

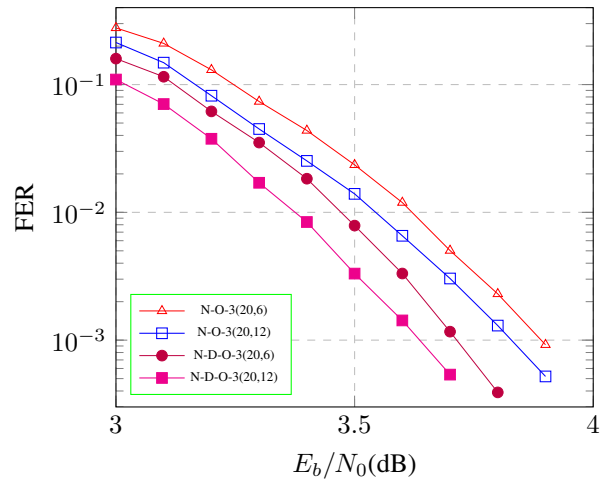


Fig. 10: Performance comparison for decoding schemes with/without DIA of (1056,880) code

For the LDPC (1056,880) code, as shown in Fig. 10, the integration of DIA assists N-D-O-3 with  $l_{pt} = 6$  to outperform the case without DIA by about 0.2dB. An additional 0.08dB gain is observed when the  $l_{pt}$  of N-D-O-3 increases to 12.

The traditional BCH (63,36) code is a high-density parity-check code with many short cycles in its code structure. As shown in Fig. 11, compared with the conventional combination N-O-1, DIA yields about a 0.1dB gain for N-D-O-1. However, this advantage diminishes gradually as the order  $\lambda_m$  increases to 3, covering fewer decoding errors of high Hamming weight than the absence of DIA. Consequently, it necessitates the

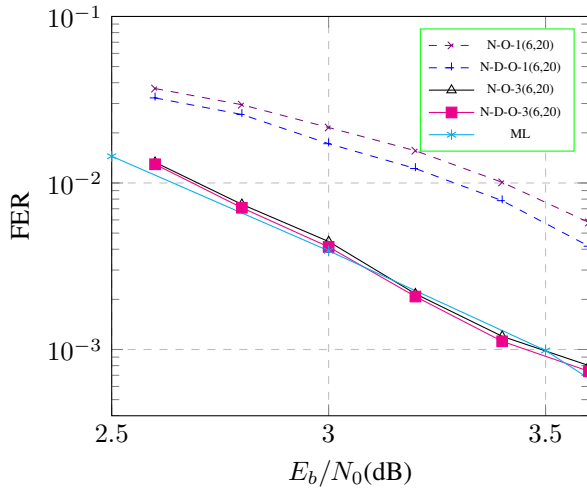


Fig. 11: FER comparison for various decoding schemes of BCH (63,36) code

tailing of the order-3 OSD to reach ML decoding for both N-O-3 and N-D-O-3 schemes. From another perspective, it was found the FER of NMS is above 0.5 in the test SNR region, thus the trajectories of its decoding errors consist of highly correlated messages, leading to the situation that DIA fails to distill and grasp the useful mode to substantially improve its estimation.

### E. Complexity Analysis

As previously mentioned, the decoding process of the conventional order- $p$  OSD follows a predetermined path composed of a comprehensive list of order patterns with Hamming weights less than or equal to  $p$ . This path is traversed sequentially in ascending order of Hamming weights. In contrast, our adaptive order- $\lambda_m$  OSD addresses the occurrences of each order pattern to determine its precedence. Furthermore, we have the flexibility to arbitrarily tailor the nominal path length  $l_{pt}$  and impose more refined constraints on the order patterns, deciding whether to include them in the decoding path. This customization results in an incomplete list of order patterns compared to the conventional OSD. Additionally, DIA demonstrates a concentration effect for the adaptive OSD by categorizing more decoding errors into its dominant order patterns.

When the surviving order patterns start generating TEPs to populate the codeword candidates list, the introduction of auxiliary criteria will play the role of executing admission or refusal judgments to prevent the list from exceeding its predefined size. The impact of this safeguarding mechanism is detailed in the next subsection.

All of these factors make it possible to adjust the trade-off between computational complexity and decoding performance. For example, in the case of the (128,64) code, despite the intensive complexity incurred by the conventional order- $p=3$  OSD, the adaptive order- $\lambda_m=3$  OSD can significantly alleviate

this situation with minimal performance loss, as elaborated in the following description.

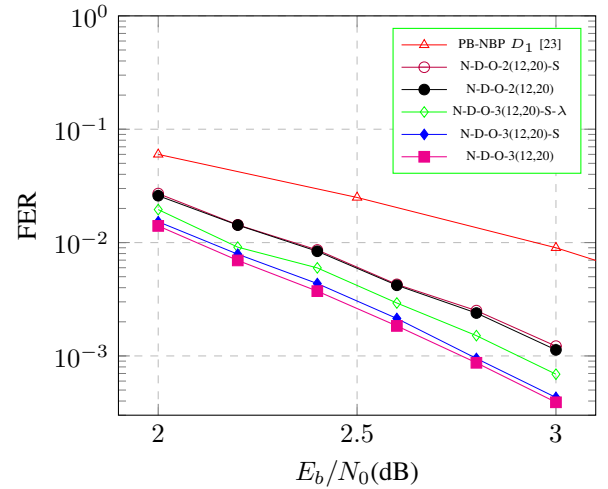


Fig. 12: FER comparison of various decoders of LDPC (128,64) code with and without the auxiliary criterion

1) *Role of Auxiliary Criterion:* The purpose of applying an auxiliary criterion is to prevent the inclusion of generated codewords related to unlikely TEPs into the candidate codewords list. This process helps save significant memory consumption and computation, such as real additions or comparisons, when selecting the best estimate among them. Naturally, our primary interest lies in understanding how the application of the auxiliary criterion impacts decoding performance and complexity.

For the (128,64) code, as depicted in Fig. 12, the decoding schemes suffixed with 'S' indicate the application of the auxiliary criterion. It can be observed that the performance variation is negligible for order-2 or 3 adaptive OSD, whether the criterion is applied or not. However, as illustrated in Table V, the introduction of the auxiliary criterion can significantly reduce OSD complexity. Specifically, throughout the waterfall SNR region, a load reduction of 1/3 and 2/3 is expected for order-2 and order-3 OSD, respectively. Similar observations hold for other codes as well. As a benchmark, despite its simplicity, PB-NBP- $D_1$  in Fig. 12 exhibits a significant performance loss compared to other schemes.

TABLE V: Comparison of the candidate codewords list size for order-2,3 OSD of LDPC (128,64) code with and without the auxiliary criterion

$\lambda_m$	Auxiliary Criterion?	2.0dB	2.2dB	2.4dB	2.6dB	2.8dB	3.0dB
2	No	2081	2081	2081	2081	2081	2081
	Yes	<b>1395</b>	<b>1415</b>	<b>1423</b>	<b>1439</b>	<b>1452</b>	<b>1461</b>
3	No	43745	43745	43745	43745	43745	43745
	Yes	<b>13601</b>	<b>13781</b>	<b>13897</b>	<b>14019</b>	<b>14150</b>	<b>14180</b>

2) *Impact of Varying Decoding Path Length and Order Pattern Constraints:* In the context of adaptive OSD, a decoding path is composed of a sequence of order patterns, each guiding the qualified TEPs to populate the codeword candidates list.

Tweaking the decoding path length  $l_{pt}$  can be employed to manage complexity, although it often comes at the cost of performance degradation. Additionally, fine-tuned constraints on potential order patterns can be utilized to determine whether to include them in the decoding path.

Assuming the absence of an auxiliary criterion, the actual size of a candidate codewords list is calculated as follows:

$$\sum_{\lambda_1=0}^{\lambda_{1m}} \sum_{\lambda_2=0}^{\lambda_{2m}} \sum_{\lambda_3=0}^{\lambda_{3m}} \binom{L_\lambda}{\lambda_1} \binom{M_\lambda}{\lambda_2} \binom{H_\lambda}{\lambda_3} \quad (10)$$

where  $L_\lambda = n_{sw}$ ,  $M_\lambda = 2n_{sw}$ , and  $H_\lambda = K - 3n_{sw}$  denote the specific sizes of three partitions of MRB, and  $[\lambda_1, \lambda_2, \lambda_3]$  represents a specific order pattern.

A closer examination of (10) reveals that different order patterns contribute vastly differently to the total sum, even with the same Hamming weight. For example, in the case of the (128,64) code, order patterns  $[3, 0, 0]$  and  $[0, 3, 0]$  contribute 4 and 56 TEPs, respectively. In contrast, the order patterns  $[1, 0, 2]$  and  $[0, 1, 2]$  contribute 5304 and 10608 TEPs, respectively. This substantial difference between order patterns in terms of the number of TEPs necessitates additional fine-tuned constraints on the combination of  $[\lambda_{1m}, \lambda_{2m}, \lambda_{3m}]$ , denoted as  $\Phi(\lambda_{1m}, \lambda_{2m}, \lambda_{3m})$ , whose contents depend on the performance and complexity requirements. For instance, in the case of order- $\lambda_m$  OSD of LDPC (128,64) code with  $n_{sw} = 4$  and  $\lambda_m = 3$ , its  $\Phi(\lambda_{1m}, \lambda_{2m}, \lambda_{3m})$  may consist of the following constraints:

$$\sum_{i=1}^3 \lambda_{im} \leq \lambda_m ; \quad \lambda_{3m} \leq 2 ; \quad \lambda_{1m} = \lambda_{2m} = 0 \text{ if } \lambda_{3m} = 2.$$

It was found that checking  $\Phi(\lambda_{1m}, \lambda_{2m}, \lambda_{3m})$  results in a list size reduction to approximately 3881~4094, which is only one-tenth of the size of the conventional OSD. This reduction comes at the cost of a 0.1dB performance loss in the waterfall SNR region, as depicted in the green FER curve of Fig. 12

Therefore, numerous trade-offs between performance and complexity can be readily achieved through varying  $l_{pt}$  and designing dedicated constraints.

### F. Computational Complexity Comparison of Various Decoders

In the case of OSD, although steps such as GE and generating the codeword candidates list involve numerous binary or logical operations, we opt not to consider them in terms of complexity analysis. Firstly, these operations are hardware-friendly. Secondly, as a postprocessing step, OSD is called upon only to address decoding errors in BP or MS variants. For instance, if the FER of the NMS is 0.1, it implies that the workload of OSD is one-tenth of that of NMS. Clearly, NMS takes on the primary decoding work, while OSD plays the auxiliary role of supplementing performance. Recognizing this, only real arithmetic operations, which dominate the complexity of various decoders, are considered hereafter.

Suppose we have a received sequence of an LDPC  $(N, K)$  codeword with  $T$  iterations of decoding, given the average

column and row weights of its  $\mathbf{H}$  as  $w_c$  and  $w_r$  respectively. The worst-case decoding complexity for some typical decoders is approximated in Table. VI.

TABLE VI: Worst-case complexity comparison per sequence of various decoding schemes for LDPC  $(N, K) = (128, 64)$  code with  $(w_c, w_r) = (4, 8)$ .

Decoders	Phases	Additions/Comparisons	Multiplications	Divisions	# of trainable
N-A-O-3(12,20)-S	NMS	$\frac{NT(3w_c+2)+}{(N-K)T(2w_r-3)}$ $\approx 31.5K$	$(N-K)T$ $\approx 0.8K$	0	1
	AID	460K~480K	1.065M FLOPs	0	537
	OSD-3	0	0	0	0
BP( $T=12$ ) [7]	-	$NT(3N-3K+1)$ $\approx 296.4K$	$NT(11N-11K-9)$ $\approx 1.068M$	$N(N-K+1)T$ $\approx 99.8K$	0
NBP( $T=12$ ) [14]	-	$NT(3N-3K+1)$ $\approx 296.4K$	$NT(11N-11K-9+2w_c)$ $\approx 1.08M$	$N(N-K+1)T$ $\approx 99.8K$	12288
PB-NBP- $D_1(T=25)$ [23]	-	$2NT(3N-3K+1)$ $\approx 1.23M$	$2NT(11N-11K-9)$ $\approx 26.7M$	$2N(N-K+1)T$ $\approx 2.49M$	28416
NBP- $D(10,4,4)(T=50)$ [24]	-	$18.2NT(3N-3K+1)$ $\approx 11.25M$	$18.2NT(11N-11K-9)$ $\approx 242.97M$	$18.2N(N-K+1)T$ $\approx 22.71M$	1553
$D_{10}$ -OSD-2( $T=25$ ) [25]	$D_{10}$	$10NT(3N-3K+1)$ $\approx 6.18M$	$10NT(11N-11K-9)T$ $\approx 133.5M$	$10N(N-K+1)T$ $\approx 12.48M$	10240
	OSD-2	69.02K	0	0	0

It can be observed that the total computational complexity of the proposed NMS-AID-OSD architecture comprises computation occurring in three constituent parts. Firstly, compared with BP or NBP, the NMS, with a single trainable parameter, requires much less computational complexity. Secondly, fulfilled via a four-layered CNN model, AID requires 537 trainable parameters. In contrast, NBP- $D(10,4,4)$  needs 1553 trainable parameters, and other NN decoders, including the SOTA  $D_{10}$ -OSD-2, require more than 10K trainable parameters. The order-3 adaptive OSD, as the last component of our architecture, requests less than 0.5M real additions or comparisons due to the effective functioning of auxiliary criteria and constraints on order patterns. Therefore, totally about 1.5M flops (defined as floating point operations) is required to process an NMS decoding error for our proposed architecture. It is slightly worse than BP or NBP decoding schemes, far better than PB-NBP- $D_1$ , NBP- $D(10,4,4)$ , or the SOTA. Therefore, as far as the average complexity per received sequence is concerned, the proposed will substantially lead the other counterparts.

### G. Elaborated Comparison with the SOTA Decoder

For LDPC (128,64) code, as shown in Fig. 7, the proposed N-D-O-3(12,20) presents a similar decoding performance as the SOTA decoder of  $D_{10}$ -OSD-2(25) [25], thus it is meaningful to compare them as well in terms of hardware complexity, computational complexity and latency, etc.

With the fact that the trainable parameters number is indicative of hardware complexity, the  $D_{10}$  part of  $D_{10}$ -OSD-2 decoder requires 10 BP-RNN structured NN models available, including 10240 trainable parameters. While the proposed NMS-DIA combination requires 538 trainable parameters for NMS and CNN models, thus much simpler than the  $D_{10}$  implementation.

In the training phase, the SOTA decoder follows a two-step process. Initially, it identifies the dominant absorbing sets of the code. Subsequently, a set of BP-RNN decoders, corresponding to the identified absorbing sets, undergoes training to effectively maximize decoding improvement. This process involves deliberately preparing a pinpointed training dataset for each decoder. In contrast, our solution streamlines the training process by eliminating the need for a specialized

training dataset, resulting in a significantly reduced training overhead.

As shown in Table. VI, surely the adaptive order-3 OSD requires far more complexity than order-2 OSD in the SOTA, but we contend that the advantage of the latter is significantly compromised by the substantial complexity of its predecessor  $D_{10}$ , which unluckily bears the primary decoding burden. Based on this fact, we can safely infer the proposed will outperform the SOTA in terms of computational complexity.

Lastly, with the recognized fact that CNN commonly responds much more promptly than RNN, in addition to a smaller setting of  $T$  for the NMS than that for BP, it can be inferred our N-D-O architecture will have a latency advantage over the SOTA decoder, thus implying a higher throughput over the latter.

In summary, in terms of the trade-off between decoding performance and complexity, the proposed architecture has become a serious competitor to any leading decoders.

## V. CONCLUSIONS AND FUTURE RESEARCH

The proposed NMS-DIA-OSD architecture aims to achieve leading decoding performance at the cost of minimal complexity. Firstly, we employed a bit-oriented deep learning model, termed DIA, to address decoding errors left by the NMS, one of the min-sum variants. This model substantially improves bit reliability estimates by drawing insights from the decoding trajectory. Following this, the codeword-oriented adaptive OSD traverses a specific decoding path composed of a list of order patterns. The goal is to secure the optimal one among the codeword candidate list, populated by the test error patterns. The size of this list is checked and managed with the assistance of fine-tuned constraints on order patterns and auxiliary criteria.

Simulations demonstrated that the proposed architecture, with high throughput, low latency, low complexity, and independence of channel knowledge, effectively boosts the decoding performance of short LDPC codes to near ML decoding. Furthermore, the flexible adjustments in the architecture offer many options for trade-offs between performance and complexity to meet the needs of various scenarios.

For longer LDPC codes, despite leading the counterparts, the proposed architecture faces the challenge of approaching ML performance given limited computational resources. The inherent complexity required to tackle the decoding of longer codes problem is not allowable. Another attempt on a traditional BCH code showed that the iterative message passing method is unable to provide informative trajectories to DIA to improve bit reliability estimation, resulting in marginal improvement in the succeeded OSD decoding.

Regarding any decoding error, we can also regard the trajectory of bits jointly involved in each parity check of  $\mathbf{H}$  as a multi-dimensional time series forecasting issue. Ensembling the estimation of each bit after traversing all the parity checks is expected to further improve bit reliability estimates. This can be deemed an extended version of DIA.

Not limited to the CNN in usage, there are surely more advanced NN structures available to implement DIA. Any off-the-shelf schemes for the time series forecasting task, such as temporal convolutional networks (TCN) [30], are tempting to play the role of constructing new bit reliability estimates.

## AVAILABILITY OF DATA

The parity check matrices of all related codes, as well as BP and ML decoding results, can be retrieved at the website [21] or [25], grateful for the efforts taken by the original authors for the code database maintenance and their generous sharing.

## ACKNOWLEDGMENTS

The authors would like to express their gratitude to Google Corporation for providing the excellent computing platforms of Colab and Kaggle online, which made it possible to debug, train, and test our models freely. Thanks are also extended to the anonymous reviewers for providing valuable feedback, contributing to the improvement of the quality of this paper.

## REFERENCES

- [1] Robert Gallager. Low-density parity-check codes. *IRE Transactions on information theory*, 8(1):21–28, 1962.
- [2] David JC MacKay and Radford M Neal. Near shannon limit performance of low density parity check codes. *Electronics letters*, 32(18):1645, 1996.
- [3] Jianguang Zhao, Farhad Zarkeshvari, and Amir H Banihashemi. On implementation of min-sum algorithm and its modifications for decoding low-density parity-check (ldpc) codes. *IEEE transactions on communications*, 53(4):549–554, 2005.
- [4] Ming Jiang, Chunming Zhao, Li Zhang, and Enyang Xu. Adaptive offset min-sum algorithm for low-density parity check codes. *IEEE communications letters*, 10(6):483–485, 2006.
- [5] Marc PC Fossorier and Shu Lin. Soft-decision decoding of linear block codes based on ordered statistics. *IEEE Transactions on Information Theory*, 41(5):1379–1396, 1995.
- [6] Marc PC Fossorier, Miodrag Mihaljevic, and Hideki Imai. Reduced complexity iterative decoding of low-density parity check codes based on belief propagation. *IEEE Transactions on communications*, 47(5):673–680, 1999.
- [7] Marc PC Fossorier. Iterative reliability-based decoding of low-density parity check codes. *IEEE Journal on selected Areas in Communications*, 19(5):908–917, 2001.
- [8] Chentao Yue, Mahyar Shirvanimoghaddam, Giyoon Park, Ok-Sun Park, Branka Vucetic, and Yonghui Li. Probability-based ordered-statistics decoding for short block codes. *IEEE Communications Letters*, 25(6):1791–1795, 2021.
- [9] Chentao Yue, Mahyar Shirvanimoghaddam, Branka Vucetic, and Yonghui Li. Ordered-statistics decoding with adaptive gaussian elimination reduction for short codes. In *2022 IEEE Globecom Workshops (GC Wkshps)*, pages 492–497. IEEE, 2022.
- [10] Baptiste Cavarec, Hasan Basri Celebi, Mats Bengtsson, and Mikael Skoglund. A learning-based approach to address complexity-reliability tradeoff in os decoders. In *2020 54th Asilomar Conference on Signals, Systems, and Computers*, pages 689–692. IEEE, 2020.
- [11] Muhammad Imran Razzak, Saeeda Naz, and Ahmad Zaib. Deep learning for medical image processing: Overview, challenges and the future. *Classification in BioApps*, pages 323–350, 2018.
- [12] Tom Young, Devamanyu Hazarika, Soujanya Poria, and Erik Cambria. Recent trends in deep learning based natural language processing. *IEEE Computational Intelligence magazine*, 13(3):55–75, 2018.
- [13] Sorin Grigorescu, Bogdan Trasnea, Tiberiu Cocias, and Gigel Macesanu. A survey of deep learning techniques for autonomous driving. *Journal of Field Robotics*, 37(3):362–386, 2020.
- [14] Eliya Nachmani, Yair Be’ery, and David Burshtein. Learning to decode linear codes using deep learning. In *2016 54th Annual Allerton Conference on Communication, Control, and Computing (Allerton)*, pages 341–346. IEEE, 2016.

- [15] Tobias Gruber, Sebastian Cammerer, Jakob Hoydis, and Stephan ten Brink. On deep learning-based channel decoding. In *2017 51st Annual Conference on Information Sciences and Systems (CISS)*, pages 1–6. IEEE, 2017.
- [16] Eliya Nachmani, Elad Marciano, Loren Lugosch, Warren J Gross, David Burshtein, and Yair Beery. Deep learning methods for improved decoding of linear codes. *IEEE Journal of Selected Topics in Signal Processing*, 12(1):119–131, 2018.
- [17] Fei Liang, Cong Shen, and Feng Wu. An iterative bp-cnn architecture for channel decoding. *IEEE Journal of Selected Topics in Signal Processing*, 12(1):144–159, 2018.
- [18] Loren Lugosch and Warren J Gross. Learning from the syndrome. In *2018 52nd Asilomar Conference on Signals, Systems, and Computers*, pages 594–598. IEEE, 2018.
- [19] Loren Peter Lugosch. *Learning algorithms for error correction*. McGill University (Canada), 2018.
- [20] Qing Wang, Shunfu Wang, Haoyu Fang, Leian Chen, Luyong Chen, and Yuzhang Guo. A model-driven deep learning method for normalized min-sum ldpc decoding. In *2020 IEEE International Conference on Communications Workshops (ICC Workshops)*, pages 1–6. IEEE, 2020.
- [21] Michael Helmling, Stefan Scholl, Florian Gensheimer, Tobias Dietz, Kira Kraft, Stefan Ruzika, and Norbert Wehn. Database of Channel Codes and ML Simulation Results. [www.uni-kl.de/channel-codes](http://www.uni-kl.de/channel-codes), 2019.
- [22] Eliya Nachmani and Yair Beery. Neural decoding with optimization of node activations. *IEEE Communications Letters*, 2022.
- [23] Andreas Buchberger, Christian Hger, Henry D Pfister, Laurent Schmalen, and Alexandre Graell i Amat. Pruning and quantizing neural belief propagation decoders. *IEEE Journal on Selected Areas in Communications*, 39(7):1957–1966, 2020.
- [24] Andreas Buchberger, Christian Hger, Henry D Pfister, Laurent Schmalen, and Alexandre Graell i Amat. Learned decimation for neural belief propagation decoders. In *ICASSP 2021-2021 IEEE International Conference on Acoustics, Speech and Signal Processing (ICASSP)*, pages 8273–8277. IEEE, 2021.
- [25] Joachim Rosseeel, Valrian Mannoni, Inbar Fijalkow, and Valentin Savin. Decoding short ldpc codes via bp-rnn diversity and reliability-based post-processing. *IEEE Transactions on Communications*, 70(12):7830–7842, 2022.
- [26] Ming Jiang, Chunming Zhao, Enyang Xu, and Li Zhang. Reliability-based iterative decoding of ldpc codes using likelihood accumulation. *IEEE communications letters*, 11(8):677–679, 2007.
- [27] Weiyang Zhang, Chentao Yue, Yonghui Li, and Branka Vucetic. Efficient near maximum-likelihood efficient near maximum-likelihood reliability-based decoding for short ldpc codes. *arXiv preprint arXiv:2306.00443*, 2023.
- [28] François Chollet et al. Keras. <https://keras.io>, 2015.
- [29] Diederik P Kingma and Jimmy Ba. Adam: A method for stochastic optimization. *arXiv preprint arXiv:1412.6980*, 2014.
- [30] Shaojie Bai, J Zico Kolter, and Vladlen Koltun. An empirical evaluation of generic convolutional and recurrent networks for sequence modeling. *arXiv preprint arXiv:1803.01271*, 2018.